UNIVERSITY OF CALIFORNIA, SAN DIEGO

Using California Reanalysis Downscaling at 10 km to Identify the Sierra Barrier Jet and Its Variability since 1950

A Thesis submitted in partial satisfaction of the requirements
for the degree Master of Science

in

Earth Sciences

by

Chang Sun

Committee in charge:

Professor Joel Norris, Chair
Daniel Cayan
Alexander Gershunov

2016

The Thesis of Chang Sun is approved and it is acceptable in quality and form for publication on microfilm and electronically:

_____

_____

_____

Chair

University of California, San Diego

2016

DEDICATION

To lost time.

TABLE OF CONTENTS

LIST OF FIGURES

LIST OF TABLES

ACKNOWLEDGEMENTS

I would like to acknowledge Professor Joel Norris for his support as chair of my committee. Throughout the entire project, his advices and assistance has proved invaluable to me.

I would also acknowledge Daniel Cayan, Alexander Gershunov and Marty Ralph for their advices and assistance during the project.

Furthermore, I would like to acknowledge Mimi Hughes, Paul Neiman and Mary Tyree for providing necessary data.

Finally, I would like to acknowledge Yaqing Wang for his unwavering support throughout the whole project.

This material currently is being prepared for submission for publication. Ms. Sun was the principal researcher/author on this paper. Sun, Chang; Norris, Joel. ”Using California Reanalysis Downscaling at 10 km to Identify the Sierra Barrier Jet and Its Variability since 1950”.

ABSTRACT OF THE THESIS

Using California Reanalysis Downscaling at 10 km to Identify the Sierra Barrier Jet and Its Variability since 1950

by

Chang Sun

Master of Science in Earth Sciences

University of California, San Diego, 2016

Professor Joel Norris, Chair

The Sierra Barrier Jet (SBJ) is a low-level jet that flows parallel to the west slope of the Sierra Nevada and affects precipitation in California during cool seasons (October to April). This study begins by evaluating the ability of California Reanalysis Downscaling at 10 km (CaRD10) to identify the SBJ by comparison to wind profiler measurements available during cool seasons from 2000 to 2010. After adjusting thresholds for SBJ identification to account for a weak negative bias in CaRD10 Sierra-parallel component (2m s^{-1}), comparison with observed wind profiler data at Chico demonstrates that CaRD10 performs quite well at detecting strong wind speed and long duration SBJ events

that are accompanied with substantial precipitation. And CaRD10 is demonstrated to reproduce seasonal cycle and interannual variability well.

Then CaRD10 is used to study the climatological variability of SBJs from 1950 to 2012 during the cool season. Although large variations among cool season months, the magnitudes of maximum Sierra-parallel component of flow are similar. Total precipitation over an individual cool season in the region north of the Central Valley is greater for those years with a greater number of SBJ events. Although experiencing substantial year-to-year variability, the average duration of SBJ events and the daily precipitation amount associated with SBJ events do exhibit statistically significant increasing trends. With simple investigation on the linkages of SBJs with (El Nino-Southern Oscillation) ENSO and Pacific Decadal Oscillation (PDO), no significant relationships are found.

Chapter 1

Introduction

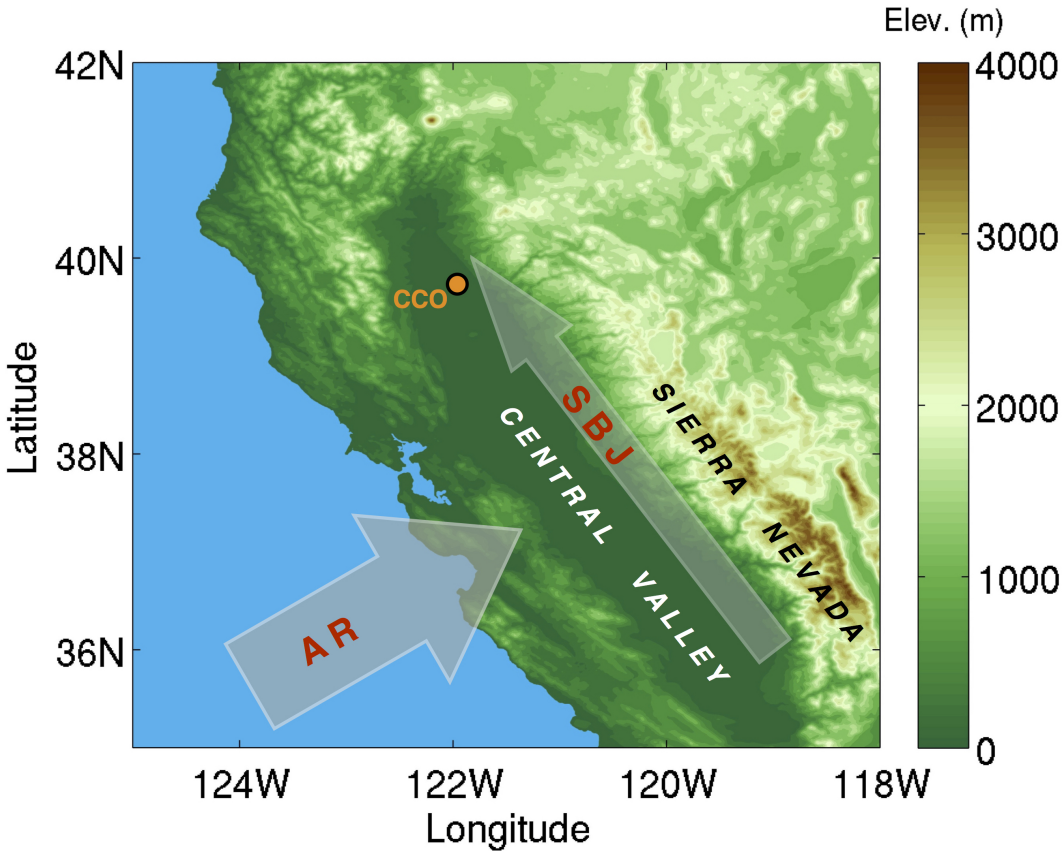

Figure 1: Topographic map of California. The location of the 915-MHz radar wind profiler at Chico (CCO) is shown in orange circle. The flow directions of the SBJ and AR are shown by arrows.

1.1 Overview of California

California is a classic Mediterranean climate region, where it is dry in summer and wet in winter. Consequently, precipitation in California mainly occurs during the cool season (October to April). Precipitation in California substantially varies from one year to another. For example, intense floods happened several times across California during the 1997-1998 cool season. Rainfall in San Francisco exceeded 130% of normal (Monteverdi and Null 2008), and floods around San Francisco Bay during January to March in 1998 forced over 11,000 people to be evacuated and caused more than $550 million in property damage (Californias Flood Future 2013). Contrastingly, during 2012 to 2014 California suffered from water shortages due to drought. In San Francisco, annual rainfall set a new lowest record (DWR 2015).

Besides interannual variation, precipitation also substantially varies spatially throughout California. Regions in the northwest part of the state can experience more than 70 inches of rainfall a year whereas the southeast part of the state receives only about 5 inches a year (Information sheet on California Precipitation 2010). This large geographical difference in rainfall is highly related to the location of mountains in California (Galewsky and Sobel 2005). The most well-known orographic effect is forced ascent of atmospheric flow encountering a mountain range. In this situation, unsaturated air parcels in the flow rise and cool adiabatically (e.g. without exchanging heat with the environment) and often become saturated due to the adiabatic cooling and decrease in atmospheric pressure with height. Considerable water vapor condensation can occur, often resulting in rainfall.

For different situations of mountains and airflows, the position and amount of rainfall may vary (Roe 2005). Neiman et al. (2002) studied precipitation over coastal mountains (under 1.5 km elevation) and found that when upslope flows were not blocked

at the foothills, precipitation was concentrated on the mountaintops. When flows were blocked, heavy precipitation occurred before the windward side of mountains (e.g. at the coast). Rain rate in coastal mountains is highly connected with upslope flow speed near the mountaintop and at the height of the low-level jet. Hughes et al. (2009) explored the linkage of precipitation with terrain slope. Under weak blocking situations, rainfall in coastal regions of Southern California increased mainly with terrain slope. But for strong blocking situations, rainfall does not vary much with terrain gradient.

Atmospheric rivers (ARs) play an important role in strong precipitation events in California. ARs are the long, narrow, low-level, and water vapor rich part of the broader warm conveyor belt within the warm sector of extratropical cyclones (Browning, 1990; Ralph et al. 2004). Floods occurring in California are highly related to AR events producing large amounts of moisture transport (Ralph et al., 2006). Recently, Kingsmill et al. (2013) reported that ARs flowing perpendicular to the Sierra Nevada Mountains were observed to occur with low-level jets flowing parallel to the range (Figure 1). These low-level jets, called Sierra Barrier Jets (SBJs), intensify the rainfall both along the Sierra windward slope and the north end of Central Valley (Neiman et al. 2013). First recorded during the Sierra Cooperative Pilot Project (SCPP; Reynolds and Dennis 1986), the SBJ is defined as a low-level jet that extends northward at least 100 km, paralleling the western slope of the Sierra Nevada. The strongest winds are found between 600 m and 1500 m above ground level and usually exceed 20 m s^{-1} (Parish 1982).

1.2 SBJ mechanism

The mechanism generating SBJs is generally understood. When a low-level atmospheric flow moves toward a mountain barrier, it tends to be blocked and decelerates

when the Froude number (Fr) is less than unity. Froude number is defined as Fr = u/hmN, where u is the ambient velocity component normal to the barrier, hm is the height of the obstacle, and N is the Brunt-Vaisala frequency. Cold air damming combined with the rise of pressure result in ageostrophic acceleration that creates a leftward airstream in the Northern Hemisphere and a stagnation point (U=0) upstream of the ridge. Under this condition, a barrier jet usually forms along the long axis of the mountain. (Pierrehumbert and Wyman 1985; Smolarkiewcz and Rotunno 1990; Galewsky and Sobel 2005; Loescher and Young 2006; Kim and Kang 2007). During the cool season, strong SBJs often develop along the windward slope of the Sierra Nevada.

In recent years, the effects of SBJs on precipitation in California have received much attention. Kim and Kang (2007) used a numerical mesoscale model to explore the association of Froude number with moisture fluxes in a winter season. They found that in the low-Fr case, precipitation in the north region of the Sierra Nevada is heavier than in the south region because the SBJ transports vast amounts of water vapor northward. Smith et al. (2010) further used a finer resolution model to document the effects of moisture fluxes conveyed by the SBJ to northern California during an AR event. Lundquist et al (2010) found a negative correlation between the orographic precipitation gradient and SBJ height based on yearly observational data. The orographic precipitation gradient increases when the SBJ is lower and accompanied by stronger westerly winds. Neiman et al. (2010) used observational wind profiles from 2000 to 2007 combined with the North American Regional Reanalysis (NARR, Mesinger et al. 2006) to study vertical characteristics of the SBJ. They also found that SBJs occur at greater frequency and higher strength during the cool season (October - April). Moreover, a substantial portion of cool-season rainfall at Chico (CCO), California, occurs during SBJ events.

1.3 Shortcoming of previous work

At present, the kinds of data used to study SBJ vertical structure are limited. The most common is wind profiler data. Although observational data can truly give the map of SBJs, wind profiler data is not available prior to 2000. Thus, it is not possible to explore decadal variability in SBJs using direct measurements. An alternative to wind measured by a profiler is wind obtained from numerical weather prediction model reanalyses. The North American Regional Reanalysis (NARR) has a much longer period than the wind profiler and can go back to the late 1979 with 32 km horizontal resolution, but Hughes et al. (2012) identified several drawbacks: a suspiciously large discrepancy in wind speed between contiguous grids and the inadequate representation of coastal mountainous terrain, both of which are caused by coarse resolution. In addition, the magnitude and direction of water vapor transport had many biases.

A higher resolution model might provide a better representation of winds over California and the SBJ. The California Reanalysis Downscaling at 10 km (CaRD10) provides output at 10 km instead of 32 km from the NARR and furthermore extends back to 1948. One major assumption of the CaRD10 modeling approach is that small-scale details are fully forced by the large scale (Kanamitsu and Kanamaru 2007). This assumption performs well when the large-scale forcing is strong, such as during the cool season when the SBJ is stronger and occurs more frequently. Despite the longer record and higher horizontal resolution of CaRD10, as well as the good adaptability to the cool season, no previous studies have yet used CaRD10 as the primary dataset for investigating SBJs. Although Hughes et al. (2012) pointed out that CaRD10 data was archived at low vertical resolution, this study will demonstrate that CaRD10 output is sufficient for identifying the occurrence of SBJs.

1.4 My work

The present study is the first to assess the ability of CaRD10 to identify SBJs based on the criteria established by Neiman et al. (2010) using wind profiler measurements. Since the modeled winds in CaRD10 are not the same as the measured winds, the SBJ identification criteria are optimized for CaRD10. In the next part, CaRD10 is evaluated in terms of how well it identifies periods during which SBJs occur, how well it reproduces the observed wind profiles during SBJ events, and whether it can identify the most important SBJ events (e.g., when heavy precipitation occurs). The seasonal cycle and interannual variability of SBJ events produced by CaRD10 is also compared with observational data. After the reliability of CaRD10 in identifying SBJ events has been demonstrated, the long record of CaRD10 is employed to study the climatology of SBJ events, how they have varied between 1950 and 2012, and whether there is any relationship between SBJ events and the El Nino-Southern Oscillation (ENSO), as well as Pacific Decadal Oscillation (PDO) phenomenon. Pacific climate modes are known to be responsible for climate variability and predictability in the region of California (Gershunov and Cayan 2003).

Chapter 2

Datasets

2.1 Wind Profiler Observations

Wind data came from 915-MHz radar wind profilers (Carter et al. 1995) at Chico (CCO, Fig. 1), which were developed by the National Oceanic and Atmospheric Administrations Earth System Research Laboratory (NOAA/ESRL). The CCO profiler is located in the northern Central Valley at 39.69N, 121.91W at an elevation of 41 m above mean sea level (MSL). The radar system transmits electromagnetic energy into the atmosphere and measures backscattered energy coming from elevations between 0.1 km and 5 km. There are three formats of wind profiler data: raw spectra data, moments data, and time-averaged data (Coulter 2005). Usually, the time-averaged data are generated using consensus averaging (Fischler and Bolles 1981). But sometimes there are obvious errors due to counterfeit measurements or Doppler velocity aliasing. The CCO profiler instead uses a verticaltemporal continuity method that can remove false measurements and fix aliased measurements. This method also provides more data in time and height (Weber et al. 1993). The profiler provides hourly mean data averaged from 2-minute data, with 100 m vertical resolution and 1 m s^{-1} accuracy in all weather conditions.

Extra quality control was implemented by visually finding the remaining outliers. Data coverage exceeds 90% up to at least 2.5 km MSL, which is sufficient for studying the SBJ (Neiman et al. 2010).

The observational data used in this paper is from 01 Oct 2000 to 30 Apr 2010. The variables include wind speed and direction for each 100-m height interval from the ground to about 4 km, a total of 38 layers.

2.2 CaRD10 Output

The California Reanalysis Downscaling at 10 km system (CaRD10) was developed at the Scripps Institution of Oceanography (SIO) (Kanamitsu and Kanamaru 2007). The main idea of CaRD10 is to obtain mesoscale details by forcing a regional model with a global analysis. Specifically, the NCEP-NCAR reanalysis (NNR; with 2.5 degree spatial grid; Kalnay et al. 1996) was dynamically downscaled with the Regional Spectral Model (RSM; Juang and Kanamitsu 1994). The RSM was from originally developed by the National Centers for Environmental Prediction (NCEP) and improved at SIO (Kanamitsu et al. 2005). It uses the optimum spectral perturbation filtering method in which the difference between the full field and the background field is calculated using spectral decomposition. The RSM uses the primitive equation system, which includes the momentum equation, thermodynamic equation, mass conservation equation, and moisture equation. In order to satisfy the system assumption that the horizontal scale is much larger than the vertical scale in combination with the fact that relatively small vertical-scale atmospheric phenomena are prevalent in California, 10 km resolution was chosen. In order to increase the accuracy of dynamical downscaling procedure, a scale-selective bias correction (SSBC) scheme is used to reduce errors at scales greater than

1000 km, which are most influential according to Kanamaru and Kanamitsu (2007a).

Another regional model in common use is the NARR. One difference between CaRD10 and the NARR is that the former did not directly use station observations to fix model forecast bias whereas the latter used data assimilation (Kanamaru and Kanamitsu 2007b). However, due to higher horizontal resolution CaRD10 simulates daily near-surface wind better than NARR. Additionally, CaRD10 reproduces diurnal oscillations of low-level wind speed well.

CaRD10 output is available at 10 km horizontal resolution and standard meteorological pressure levels (1000hPa, 925 hPa, 850 hPa, 700 hPa, 600 hPa, 500 hPa, 400 hPa, 300 hPa, 250 hPa, 200 hPa 150 hPa, 100 hPa, 70 hPa, 50 hPa, 30 hPa, 20 hPa and 10 hPa). Four pressure levels occur under an elevation of 3 km (1000 hPa, 925 hPa, 850 hPa, and 700 hPa), the layer of the atmosphere in which the SBJ occurs. Although CaRD10 output is available for 1948-2012, only data starting in 1950 are used in this study because precipitation data are available only from 1950. This study did not use precipitation output from CaRD10 since high-frequency rainfall is among the least realistic variables in dynamical atmospheric models.

2.3 L13 Dataset

The present study uses L13 precipitation data (Livneh et al. 2013) gridded at 1/16 degree spatial resolution based on precipitation observations from National Climatic Data Center (NCDC) Cooperative Observer (COOP) stations. Since the station measurements are reported as an accumulation of precipitation over the 24 hours prior to observation time, the daily precipitation amount was distributed linearly between days according to the recording time of the observation. For example, if the rainfall gauge reports at 0600

local standard time, 6/24 (e.g., 1/4) of the daily precipitation amount would be attributed to that local day and the rest assigned to the previous local day. Station measurements were gridded at 1/16 degree resolution using the synergraphic mapping system (SYMAP) algorithm (Shepard 1984; Widmann and Bretherton 2000), along with quality control (QC) flags. The gridded values were furthermore adjusted to be consistent with the long term mean of the Parameter-Elevation Regressions on Independent Slopes Model (PRISM; Daly et al. 1994). The method calculated the ratios of PRISM monthly average precipitation during 1961-1990 to the gridded monthly average station precipitation during the same time for each grid, then the gridded precipitation data were scaled based on the 12 ratios. Due to underestimation by PRISM in snow-dominated areas (Goodison et al. 1998), the L13 inherits the negative errors of PRISM in some places. The data used in this study are from 1950 to 2012.

Chapter 3

Criteria to identify SBJ

This section introduces the criteria to identify SBJ events in CaRD10 with a comparison to previous studies. The vertical wind structure of SBJs and precipitation associated with SBJs are illustrated. I introduce some metrics to evaluate how well CaRD10 identifies SBJ events in comparison to profiler measurements, and we then adjust threshold criteria for SJB identification to maximize the match with profiler measurements.

Non-cool season data are not used in this study. Besides above three datasets, I also use the start time and end time (including date and hour) for each SBJ event identified by Hughes et al (2012) during the cool seasons (excluding April) of 2000-2010. SBJ events during April are filled in with those identified by Neiman et al. (2010), albeit only for 2000 to 2007.

3.1 Observational definition of the SBJ

Many previous studies used criteria defined by Neiman et al (2010) to identify SBJs with wind profiler data. To begin with, all wind analyses are based on a terrain-

relative coordinate system in which the axes are rotated 20 counterclockwise from the cardinal directions. In this case the positive V component is parallel to the Sierra Nevada range (directed from 160 to 340, where 0 is north), and the positive U component is orthogonal to the Sierra Nevada range (directed from 250 to 70). Then the V wind profile data are examined to determine whether they satisfy four requirements to be a SBJ event. 1) Hourly averaged wind profile must have a relative maximum in the V component of the flow greater than 12 m s^{-1} at an elevation below 3 km MSL. If more than one relative maximum occurs, the largest maximum (Vmax) is taken as the SBJ in that profile. 2) V must decrease by more than 2 m s^{-1} between the altitude of Vmax and 3 km MSL. 3) Vmax must occur at or higher than 200 m to ensure shallow surface-based flows will not affect SBJ identification. Furthermore, data should exist between 200 m and the Vmax height. 4) At least 8 consecutive hourly wind profiles should satisfy the above criteria.

Figure 2 provides a sense of the vertical structure of SBJs identified by Neiman

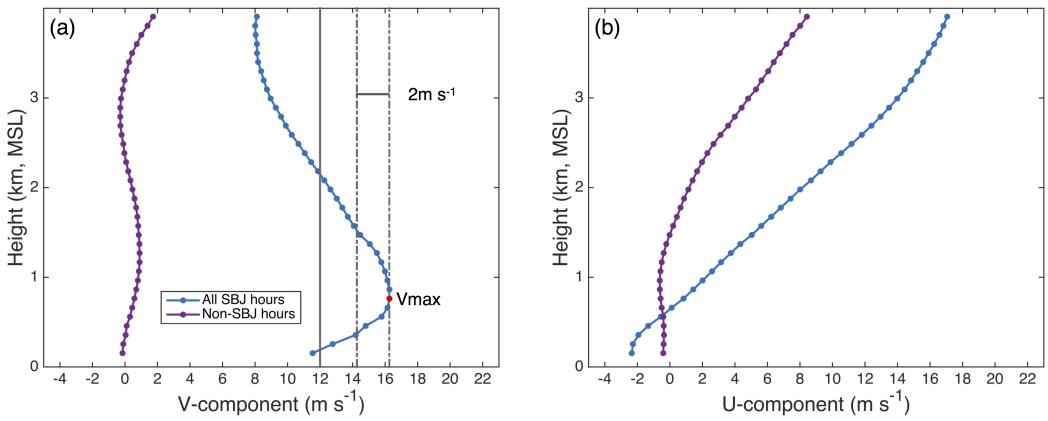

Figure 2: Average wind profiles at CCO reported by the wind profiler.(a) V-component (m s^{-1}) and (b) U-component (m s^{-1}) for SBJ hours (blue dot line) and Non-SBJ hours (purple dot line). The red dot marks the layer and maximum amplitude of V. The vertical solid grey line in (a) is the minimum threshold of Vmax for SBJ identification, and the difference between two vertical dashed grey lines is 2 m s^{-1}, the minimum threshold for the difference between Vmax and V at 3 km MSL.

et al. (2010) using observations from 2000 to 2010. The magnitude of the average

V-component for SBJ events exceeds 16 m s^{-1} at about 760 m MSL, much larger than the minimum threshold of 12 m s^{-1}. Moreover, the average speed difference between Vmax and V at 3 km MSL reaches 7.5 m s^{-1}, also much larger than the minimum threshold of 2 m s^{-1}. The mean magnitude of V during Non-SBJ hours is much lower and there is no intense wind shear. The U-component during SBJ hours increases linearly and rapidly with height, with an increase of about 16 m s^{-1} from surface to 3 km MSL. For the Non-SBJ hours, U does not increase as much with height as it does during SBJ times.

Figure 3 shows the spatial distribution of daily precipitation amount averaged

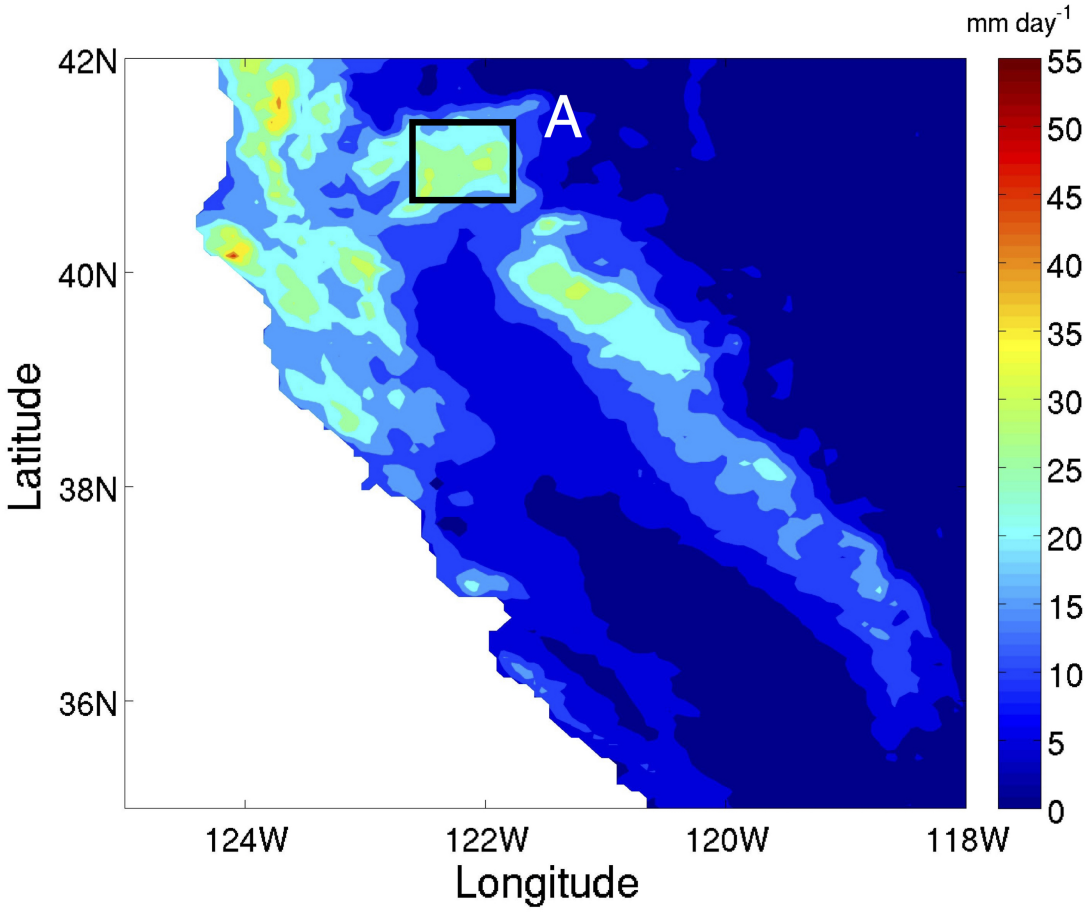

Figure 3: Average daily precipitation map for SBJ hours identified by the wind profiler from 2000 to 2010. The black rectangular is Region A (40.6 41.4N, 121.8 122.6W).

over all days on which Hughes et al. (2012) combined with Neiman et al. (2010) identify

SBJs. Recall that SBJs transport water vapor northward and greatly enhance precipitation at the north end of the Central Valley (Kim and Kang 2007; Smith et al. 2010; Neiman et al. 2010). Correspondingly, it can be seen in Fig. 3 that most parts of that region receive on average precipitation exceeding 25 mm per day with maxima nearly reaching 35 mm per day. In order to study the region at the north end of the Central Valley in more detail, we select the area within 40.6 41.4N, 121.8 122.6W for further investigation (rectangle displayed in Fig. 3). We call the rectangular area Region A.

3.2 CaRD10 definition of SBJ

Since CaRD10 only provides winds at standard meteorological pressure levels (e.g. 1000 hPa, 925 hPa, 850 hPa, 700 hPa and 600 hPa), SBJs are identified by wind data at only four or five elevations (data at 600 hPa are interpolated in cases where the altitude at 700 hPa is below 3 km MSL). Hourly wind data for identifying SBJs are obtained from the closest CaRD10 grid point to CCO. The investigation for whether this point is the most appropriate one to be used is at the end of this section. In order to test the ability of CaRD10 to identify SBJs according to the criteria of Neimen et al. (2010), CaRD10 output is examined from 2000 to 2010, the same period for which wind profiler data are available. Every hour during the time period is classified into one of four categories: hours identified as SBJ occurrence by both CaRD10 and the observations (Matched SBJ hours), hours identified as SBJ occurrence by the observations but not CaRD10 (Obs-only hours), hours identified as SBJ occurrence by CaRD10 but not the observations (CaRD10-only hours), and hours that neither CaRD10 nor the observations identify as SBJ occurrence (Non-SBJ hours).

Figure 4 displays average V-component wind profiles for each of the four cate-

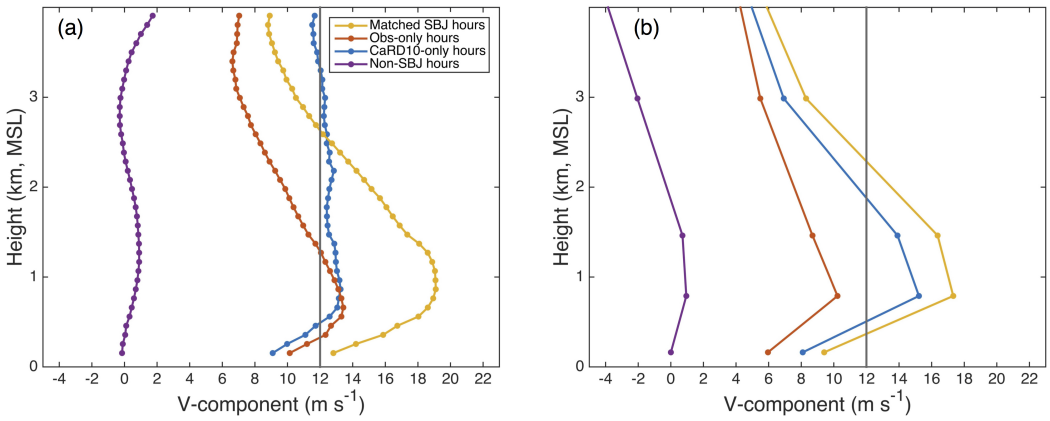

Figure 4: Average V-component of (a) wind profiler at CCO and (b) CaRD10s closest grid point to CCO based on original criteria. Matched SBJ hours (yellow line), Obs-only hours (red line), CaRD10-only hours (blue line) and non-SBJ hours (purple line) from 2000 to 2010. The vertical solid grey lines show the Vmax threshold for SBJ identification (12 m s^{-1}).

gories. For the matched SBJ hours, the Vmax appears around 1 km MSL and exceeds 19 m s^{-1}, passing the threshold. The difference in wind speed between the Vmax level and 3 km MSL is larger than 9 m s^{-1}, which also greatly surpasses the threshold. It is obvious that both Vmax and wind shear are strongest during matched SBJ hours among the four categories. The Vmax height simulated by CaRD10 is close to the observed height, and the Vmax speed surpasses 17 m s^{-1}, about 2 m s^{-1} weaker than observations. Additionally, the wind shear shown by CaRD10 is similar to the observed wind shear. Overall, CaRD10 reproduces all characteristics well during the Matched SBJ hours.

For the Obs-only hours, the vertical structure of the observed V-component is similar to the Matched-SBJ hours, but Vmax has weaker wind speed (13 m s^{-1}) and occurs at a lower height (roughly 0.6 km MSL). Also, the observed wind shear is smaller with only a 7 m s^{-1} difference between the height of Vmax and 3 km MSL. The differences between Obs-only and Matched profiles indicate that Obs-only SBJs are weaker than Matched SBJs. CaRD10 generally shows these differences as well, but due to its negative wind speed bias, the Vmax speed is only 10 m s^{-1} and does not exceed the 12

m s^{-1} threshold. This is the most likely reason that CaRD10 did not identify these hours as SBJs. The CaRD10 V-component wind speed difference between the Vmax level and 3 km MSL is only 5 m s^{-1}.

CaRD10 produced weaker Vmax and wind shear compared with observations for Matched SBJ hours and Obs-only hours, but for the times incorrectly identified as SBJs by CaRD10, the Vmax speed is slightly higher than observed. The most significant difference between observations and CaRD10 for CaRD10-only profiles is that CaRD10 shows the typical wind shear characteristic of the SBJ whereas the average observed profile exhibits little change of wind speed with height. This is the reason why these hours were not identified as SBJs in the observations even though the Vmax speed slightly exceeded the threshold. Also, the overestimated Vmax during CaRD10-only hours may explain the generally larger amplitude of CaRD10 relative to observations during SBJ periods identified by CaRD10 in the study of Hughes et al. (2012). The average magnitude of the V-component speed during Non-SBJ hours is small for both CaRD10 and the observations. This is expected as northward winds tend to occur as often as southward winds as extratropical cyclones pass through and thus tend to cancel in the mean.

According to the above comparison, CaRD10 has a small negative bias in V-component speed, suggesting that new thresholds may yield more accurate identification of SBJs by CaRD10. In order to measure the ability of other CaRD10 thresholds to identify SBJ events, three indices are introduced. They are the probability of detection (POD), the false alarm ratio (FAR), and the critical success index (CSI). The POD is an index that measures the ability to predict true events (a hit). The FAR is an index that measures the frequency of incorrectly predicting an event that did not occur (a false alarm). It is also possible to fail to predict an event that did occur (a miss). The CSI is a comprehensive index that considers both the POD and the FAR. The CSI is the most

important metric.

$$POD = \frac{hits}{hits + misses}$$

$$FAR = \frac{falsealarms}{hits + falsealarms}$$

$$CSI = \frac{hits}{hits + misses + falsealarms}$$

Here hits, misses, and false alarms correspond to Matched SBJ days, Obs-only days, and CaRD10-only days, respectively. Application of different thresholds of Vmax (originally 12 m s^{-1}) and wind shear (originally 2 m s^{-1}) may yield higher values of CSI, particularly for smaller thresholds due to the negative bias of the CaRD10 V-component speed.

Table 1: POD for different SBJ Vmax thresholds (column, m s^{-1}) and wind shear thresholds (row, m s^{-1}) from 2000 to 2010

	9	9.5	10	10.5	11	11.5	12	12.5
0.5	82.7%	81.1%	78.9%	76.7%	72.3%	70.7%	65.2%	61.6%
0.8	81.6%	80.0%	77.8%	75.6%	71.0%	69.3%	63.8%	60.3%
1.0	81.6%	80.0%	77.8%	70.7%	71.0%	69.3%	63.8%	60.3%
1.2	81.4%	79.7%	77.3%	75.3%	70.4%	68.5%	63.0%	59.5%
1.5	80.6%	78.9%	76.4%	74.3%	69.3%	67.1%	61.6%	58.1%
1.8	78.6%	7.0%	74.5%	72.1%	67.1%	64.7%	60.3%	57.0%
2.0	76.7%	74.8%	72.6%	70.4%	66.3%	64.1%	59.7%	56.7%
2.5	75.1%	73.4%	71.2%	68.8%	64.4%	63.0%	58.9%	55.6%

The values for different thresholds of the three indices are shown in Tables 1-3.

Table 2: FAR for different SBJ Vmax thresholds (column, m s^{-1}) and wind shear thresholds (row, m s^{-1}) from 2000 to 2010.

	9	9.5	10	10.5	11	11.5	12	12.5
0.5	36.3%	34.4%	32.1%	27.5%	24.6%	22.5%	21.2%	18.2%
0.8	35.5%	33.5%	30.9%	26.8%	24.3%	22.2%	21.0%	17.9%
1.0	34.8%	32.6%	30.1%	26.0%	23.0%	21.2%	20.2%	17.6%
1.2	34.6%	32.2%	29.5%	25.7%	22.8%	21.1%	20.1%	17.8%
1.5	34.1%	31.6%	28.8%	25.6%	22.4%	21.2%	20.2%	17.8%
1.8	33.4%	31.1%	28.2%	24.9%	22.2%	21.1%	19.4%	17.5%
2.0	33.7%	31.2%	28.2%	25.1%	22.2%	21.2%	19.6%	17.5%
2.5	33.2%	30.9%	27.8%	24.6%	21.7%	20.1%	18.6%	16.8%

Table 3: CSI for different SBJ Vmax thresholds (column, m s^{-1}) and wind shear thresholds (row, m s^{-1}) from 2000 to 2010

	9	9.5	10	10.5	11	11.5	12	12.5
0.5	56.2%	56.9%	57.5%	59.5%	58.5%	58.6%	55.5%	54.2%
0.8	56.3%	57.0%	57.7%	59.2%	57.8%	57.9%	54.6%	53.3%
1.0	56.9%	57.7%	58.3%	59.7%	58.4%	58.4%	55.0%	53.4%
1.2	56.9%	57.9%	58.4%	59.8%	58.3%	57.9%	54.4%	52.7%
1.5	56.9%	57.8%	58.4%	59.2%	57.8%	56.8%	53.3%	51.6%
1.8	56.4%	57.1%	57.6%	58.2%	56.3%	55.1%	52.6%	50.9%
2.0	55.2%	55.8%	56.5%	57.0%	55.8%	54.7%	52.2%	50.6%
2.5	54.7%	55.3%	55.9%	56.2%	54.7%	54.4%	51.9%	50.0%

The POD, FAR, and CSI for the original criteria is 59.7%, 19.6% and 52.2%, respectively. Both the POD and FAR generally increase with the decreasing threshold values for Vmax and wind shear, with maximum values at smallest thresholds (Tables 1 and 2). This indicates that CaRD10 identifies more observed SBJs with a lower threshold, but also falsely identifies more SBJs that were not observed. It is hard to decide the best threshold only looking at the POD and FAR. Since CSI is the combination of POD and FAR, it is better. Unlike the nearly monotonic relationship for POD and FAR seen in Tables 1 and 2, CSI rises with decreasing threshold first and then drops (Table 3). It achieves a maximum value of 59.8% when the Vmax threshold equals 10.5 m s^{-1} and the wind shear threshold

equals 1.2 m s^{-1}. At these thresholds, POD equals 75.3% and FAR equals 25.7%.

Since the most important SBJ events are those that occur with heavy precipitation, it is suitable to modify the three indices so that they are weighted by spatially averaged daily rainfall amount in Region A. For simplicity, weighted CSI, POD, and FAR are called WCSI, WPOD, and WFAR. Because precipitation data are provided in terms of daily averages, SBJ events must be identified in terms of days rather than hours. When any day includes at least on hour during which a SBJ is identified, it is counted as a SBJ day.

$$WPOD = \frac{\sum precipitation_{hits}}{\sum precipitation_{hits} + \sum precipitation_{misses}}$$

$$WFAR = \frac{\sum precipitation_{falsealarms}}{\sum precipitation_{hits} + \sum precipitation_{falsealarms}}$$

$$WCSI = \frac{\sum precipitation_{hits}}{\sum precipitation_{hits} + \sum precipitation_{misses} + \sum precipitation_{falsealarms}}$$

Here precipitationhits, precipitationmisses, and precipitationfalsealarms correspond to precipitation during Matched SBJ days, Obs-only days, and CaRD10-only days, respectively.

Tables 4-6 show WPOD, WFAR, and WCSI indices, respectively. The relative distributions of values for weighted indices are similar to those for unweighted indices, but the absolute values are higher. The thresholds for which precipitation-weighted CSI is maximum are 10.5 m s^{-1} for Vmax and 1.2 m s^{-1} for wind shear, and values

Table 4: POD for different SBJ Vmax thresholds (column, m s^{-1}) and wind shear thresholds (row, m s^{-1}) from 2000 to 2010 calculated with weighting by precipitation amount in Region A.

	9	9.5	10	10.5	11	11.5	12	12.5
0.5	91.0%	90.3%	89.2%	87.5%	84.5%	83.3%	79.5%	76.4%
0.8	90.1%	89.4%	88.3%	86.5%	83.3%	82.1%	78.2%	75.2%
1.0	90.1%	89.4%	88.3%	86.5%	83.0%	82.1%	78.2%	75.2%
1.2	89.8%	89.1%	87.7%	86.2%	82.8%	81.0%	77.1%	74.1%
1.5	89.0%	88.3%	86.9%	85.2%	81.6%	80.1%	76.3%	72.9%
1.8	87.1%	86.3%	85.0%	82.9%	79.3%	77.9%	75.2%	71.9%
2.0	85.5%	84.4%	83.3%	81.5%	78.5%	77.1%	74.4%	71.4%
2.5	84.3%	83.3%	82.2%	80.2%	76.9%	76.0%	73.5%	69.9%

Table 5: FAR for different SBJ Vmax thresholds (column, m s^{-1}) and wind shear thresholds (row, m s^{-1}) from 2000 to 2010 calculated with weighting by precipitation amount in Region A.

	9	9.5	10	10.5	11	11.5	12	12.5
0.5	21.0%	20.0%	18.8%	16.7%	15.2%	14.7%	13.6%	12.1%
0.8	20.3%	19.2%	17.9%	15.9%	14.8%	14.2%	13.2%	11.6%
1.0	19.9%	18.8%	17.5%	15.6%	14.2%	13.9%	12.8%	11.5%
1.2	19.8%	18.6%	17.4%	15.5%	14.1%	13.9%	12.9%	11.7%
1.5	19.2%	18.1%	16.9%	15.4%	14.0%	13.8%	12.7%	11.5%
1.8	19.4%	18.3%	17.0%	15.5%	14.4%	14.1%	12.8%	11.6%
2.0	19.6%	18.3%	17.0%	15.6%	14.3%	14.2%	12.9%	11.6%
2.5	19.0%	17.8%	16.4%	14.9%	13.6%	13.1%	11.8%	11.0%

of WCSI, WPOD, and WFAR are 74.4%, 86.2%, and 15.5%, respectively. Compared with the unweighted indices, WCSI and WPDO both increase by more than 10% and WFAR decreases by 10%. The changes indicate that rainfall is small during periods when CaRD10 fails to identify a SBJ or falsely identifies a SBJ. This characteristic is discussed more in a later section.

Since CSI has maximum value and WCSI has the second-greatest value at Vmax equaling 10.5 m s^{-1} and wind shear equaling 1.2 m s^{-1}, these thresholds are chosen for

Table 6: CSI for different SBJ Vmax thresholds (column, m s^{-1}) and wind shear thresholds (row, m s^{-1}) from 2000 to 2010 calculated with weighting by precipitation amount in Region A.

	9	9.5	10	10.5	11	11.5	12	12.5
0.5	73.3%	73.7%	74.0%	74.5%	73.4%	72.8%	70.6%	69.2%
0.8	73.3%	73.7%	74.0%	74.4%	72.8%	72.2%	69.9%	68.4%
1.0	73.6%	74.1%	74.3%	74.6%	73.0%	72.5%	70.2%	68.5%
1.2	73.5%	74.1%	74.0%	74.4%	72.9%	71.6%	69.3%	67.5%
1.5	73.4%	73.9%	73.9%	73.8%	72.0%	71.0%	68.6%	66.6%
1.8	72.0%	72.4%	72.3%	72.0%	70.0%	69.1%	67.7%	65.7%
2.0	70.8%	71.0%	71.2%	70.9%	69.5%	68.4%	67.0%	65.3%
2.5	70.3%	70.6%	70.7%	70.3%	68.6%	68.2%	66.9%	64.3%

CaRD10 for the rest of the analysis. Specifically, the CaRD10 hourly wind profile must have a Vmax value greater than 10.5 m s^{-1} at an elevation below 3 km MSL, and the difference in wind speed between the height of Vmax and 3 km MSL must decrease by more than 1.2 m s^{-1}. The third and fourth requirements of original criteria remain the same, and the thresholds for the observations remain the same.

Besides the adjustment of thresholds, other grid points besides the one closest to CCO are tested to see if they produce more accurate identification of SBJs. Figures 5 and 6 show the spatial distribution of CSI, POD, and FAR values (Fig. 5) and WCSI, WPOD, and WFAR values (Fig. 6) along the Sierra Nevada. The CSI and WCSI increase going northward and are maximum at the point of CCO. The POD and WPOD also present similar spatial distributions, with maximum values very close to CCO. For FAR and WFAR, though, the minimum is at the south end of test region, but overall they do not differ much. Consequently, the grid point closest to CCO appears to be the most suitable location with which to identify SBJs from CaRD10 winds.

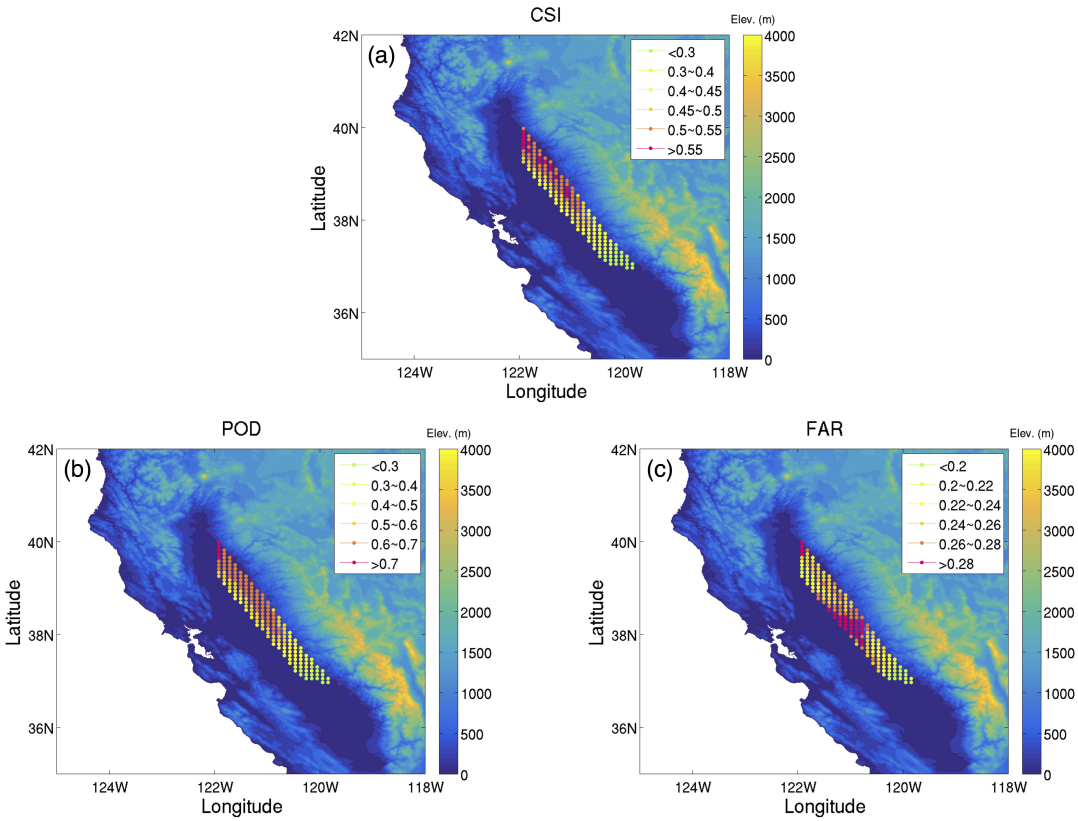

Figure 5: (a) CSI (b) POD and (c) FAR for CaRD10 grid points along the western slope of the Sierra Nevada with SBJ Vmax threshold = 10.5 m s^{-1}, wind shear threshold = 1.2m s^{-1}.

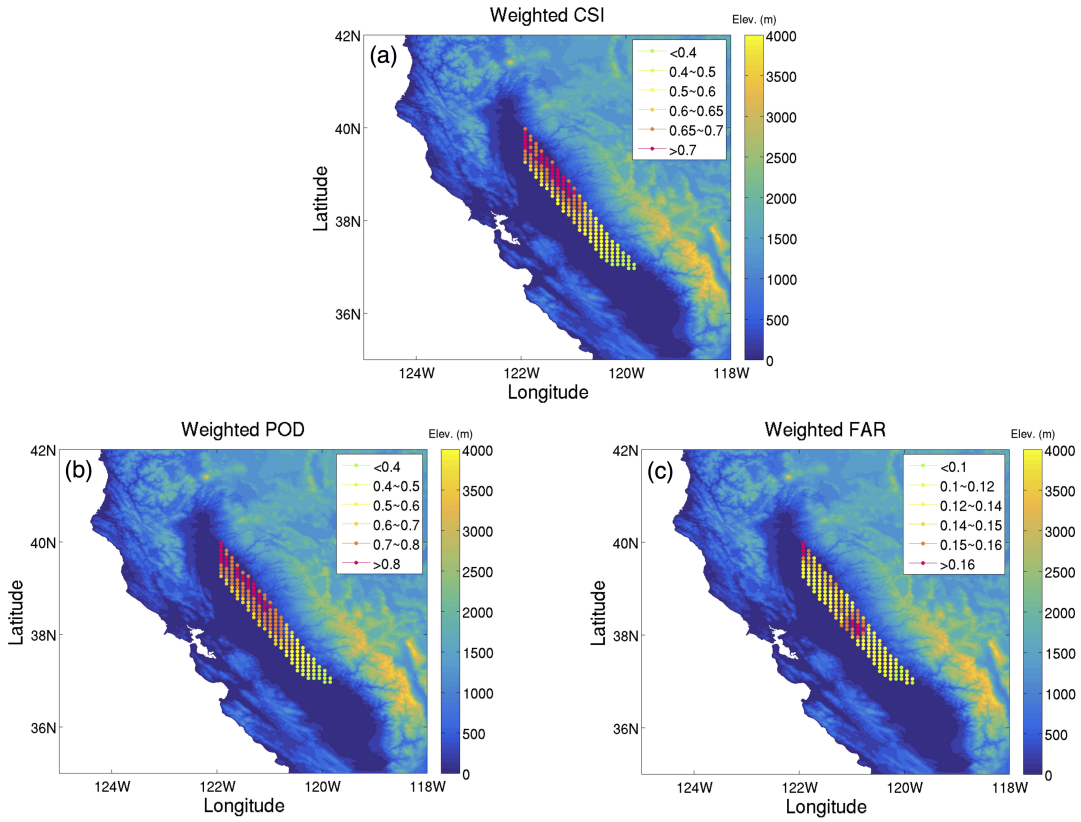

Figure 6: (a) Weighted CSI (b) Weighted POD and (c) Weighted FAR for CaRD10 grid points along the western slope of the Sierra Nevada with SBJ Vmax threshold = 10.5 m s^{-1}, wind shear threshold = 1.2m s^{-1}.

Chapter 4

Analysis

4.1 Evaluation of CaRD10

This part will assess the ability of CaRD10 to identify SBJ events through comparison of CaRD10, with wind profiles, SBJ period and precipitation first.

Using adjusted thresholds of SBJ identification, wind profiles of observations

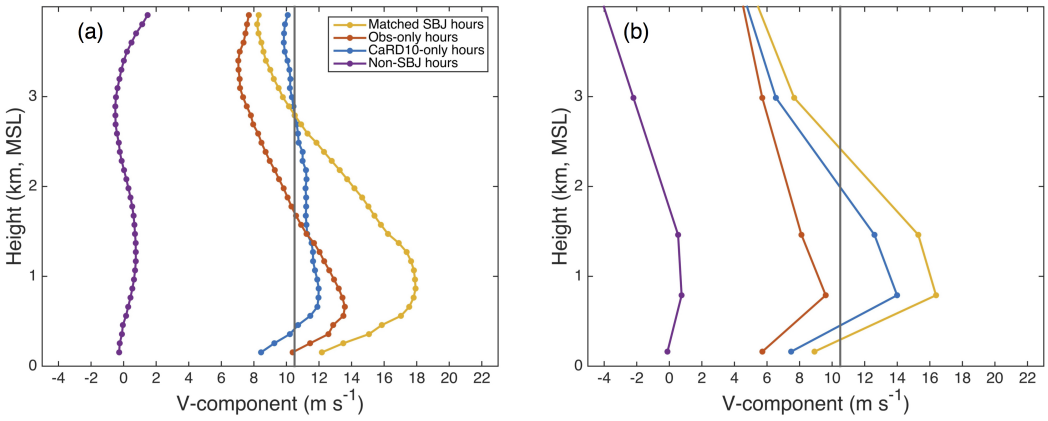

Figure 7: Average V-component of (a) wind profiler at CCO and (b) CaRD10s closest grid point to CCO based on adjusted criteria. Matched SBJ hours (yellow line), Obs-only hours (red line), CaRD10-only hours (blue line) and non-SBJ hours (purple line) from water year 2001 to 2010. The vertical solid grey lines show the Vmax threshold for CaRD10 SBJ identification. (10.5 m s^{-1}).

and CaRD10 are shown in Fig. 7. After decreasing the Vmax and wind shear threshold, more hours with relatively weak SBJs are identified by CaRD10 and counted in the Matched-SBJ hours wind profile, causing a decrease of Vmax in both observations and CaRD10 wind profiles. The observed wind profile of Obs-only hours maintains large a Vmax that exceeds 12 m s^{-1} whereas CaRD10 still shows low Vmax speed, indicating that CaRD10 has a large negative bias in V-component speeds for those hours. The drop of Vmax for CaRD10-only hours results from the lower threshold since hours that used to not be considered to have SBJs are now considered to have SBJs. Although CaRD10 has a negative bias for some weak SBJs and the wrong vertical structure for some actual non-SBJ hours, the substantial similarities of CaRD10 and observed wind profiles during matched-SBJ hours certify that CaRD10 can identify those SBJS with large values of Vmax and wind shear.

Figure 8 displays how well CaRD10 identifies those days on which the ob-

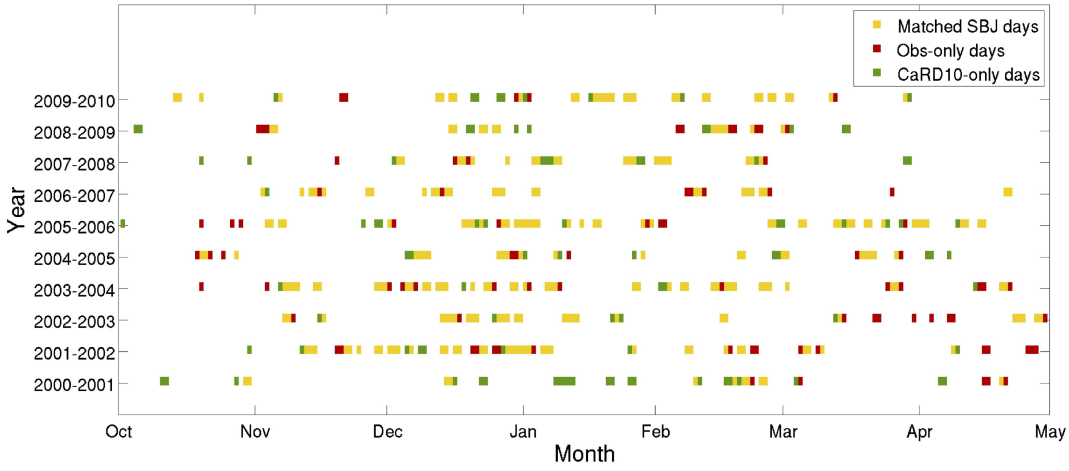

Figure 8: SBJ time for Matched SBJ days (yellow square), Obs-only days (red square) and CaRD10-only days (green square) from 2000 to 2010.

servations identify SBJ occurrence during the cool seasons for the years 2000 through 2010. Yellow, red, and green squares indicate days on which both observations and CaRD10 identify SBJs, only observations identify SBJs, and only CaRD10 identifies

SBJs, respectively. Since data for April 2008-2010 are excluded, SBJ periods are absent for that time. The domination of yellow squares demonstrates that CaRD10 can recognize most SBJs. Also, the yellow squares show high continuity, meaning that Matched days have SBJ events with longer durations than Obs-only and CaRD10-only days.

It is also of interest to determine how well CaRD10 identifies SBJs that con-

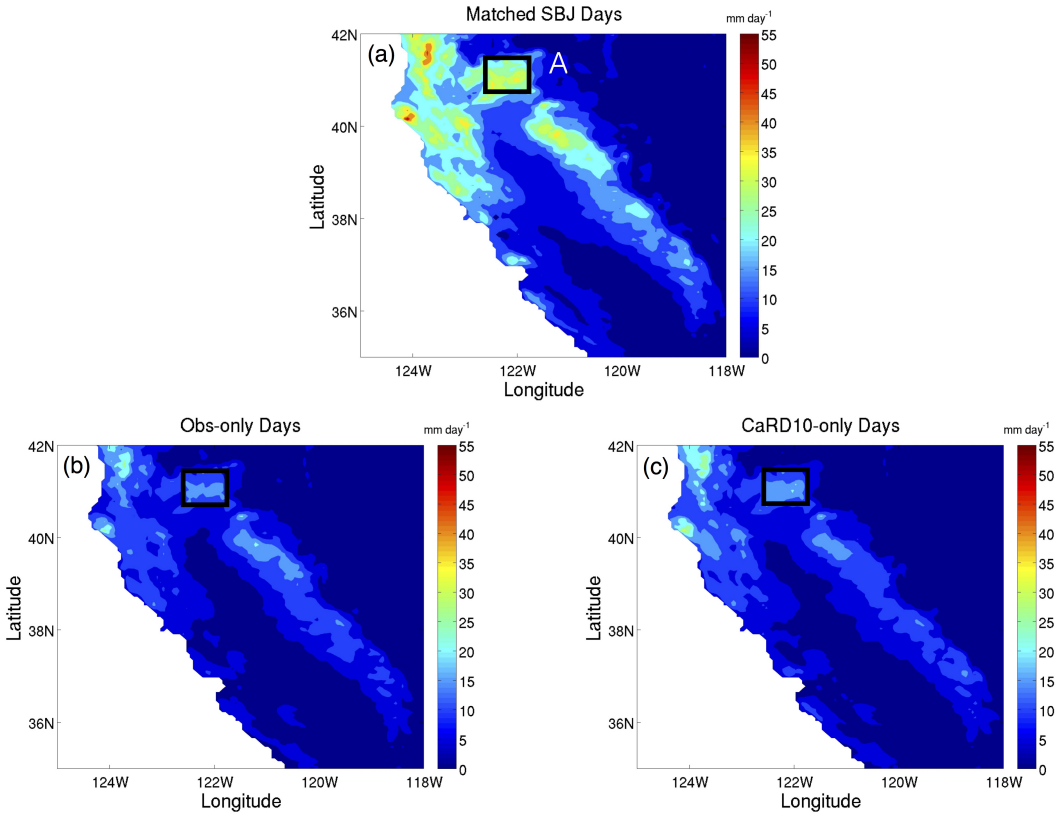

Figure 9: Average precipitation map during (a) Matched SBJ days (b) Obs-only days, (c) CaRD10-only days from 2000 to 2010. The black rectangular is region A (40.6N 41.4N, 121.8W 122.6W).

tribute substantially to precipitation. Accordingly, Fig. 9 shows the spatial distribution of average daily precipitation map for days on which both observations and CaRD10 identify SBJs, only observations identify SBJs, and only CaRD10 identifies SBJs. It is obvious that strong precipitation occurs on the SBJ days identified by both observations and CaRD10. Precipitation in northern California is much stronger than in southern

California, exceeding 55 mm per day in some areas. For Matched SBJ days, precipitation in Region A is about 30 mm per day, but much less precipitation occurs on Obs-only and CaRD10-only SBJ days, indicating that SBJ days missed or falsely identified by CaRD10 are not important contributors to precipitation.

To further investigate the importance of precipitation during Matched SBJ days

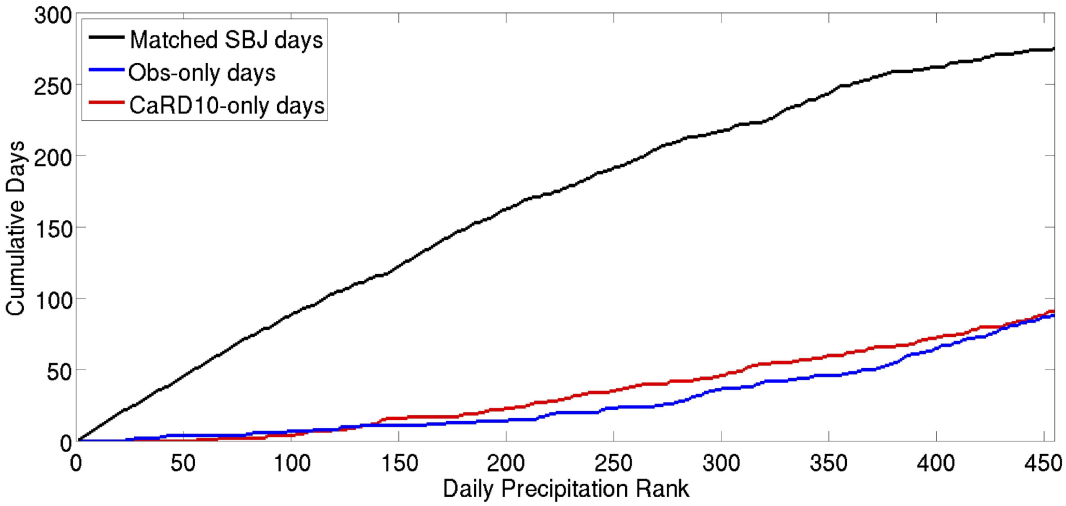

Figure 10: Cumulative precipitation days stairs. Cumulative days for Matched SBJ days (black line), Obs-only days (blue line) and CaRD10-only days (red line) starting from the most precipitation day to the least precipitation day.

in Region A, I ranked days according how much spatially averaged daily precipitation occurred in Region A among all days identified as SBJs whether by observations or CaRD10 or both. According to the accumulated ranked precipitation days [Fig. 10], Matched-SBJ days completely dominate the days on which the greatest amount of precipitation occurs. For example, 89 out of the top 100 of ranked precipitation days are identified as having SBJs by both CaRD10 and observations. This provides evidence that CaRD10 can identify SBJs that occur with heavy precipitation.

Comparison of the seasonal cycle and interannual variability with respect to SBJ events/days, Vmax, and precipitation over Region A provides an additional evaluation for CaRD10. Figure 11 gives us a sense of how well CaRD10 reproduces the observed

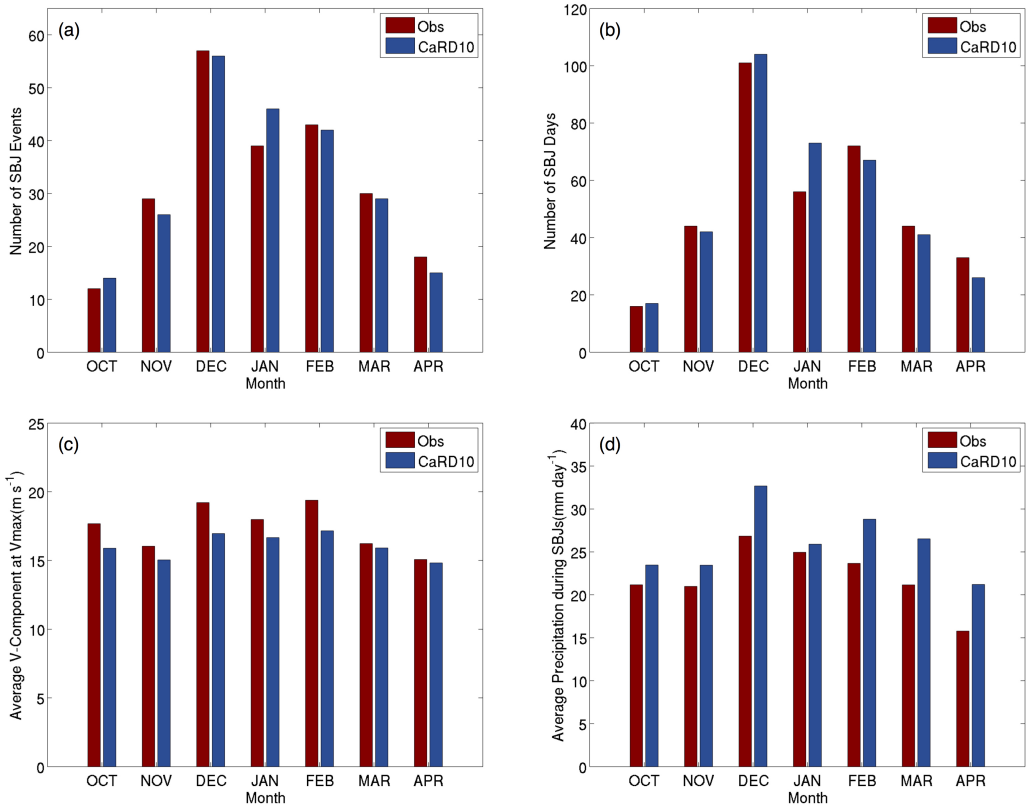

Figure 11: Cool season monthly distributions of observed at CCO and CaRD10 at the grid closest to CCO from 2000 to 2010. (a) Number of SBJ events, (b) Number of SBJ days, (c) Average V-component at Vmax (m s^{-1}) and (d) Average precipitation of Region A during SBJs. Data include 2000 to 2007, October to April and 2008 to 2010, October to March.

seasonal variation of SBJ frequency. The greatest number of SBJ events and days happen in December, totaling almost 60 events and 100 days in ten years. CaRD10 shows this characteristic well in December, and reports a similar number of SBJ events and days in other cool-season months, except January. In January, CaRD10 wrongly identifies 10 more SBJ events and 17 more days during 2000-2010 than the observations. For the magnitude of Vmax, CaRD10 matches the observations well, with only a small negative bias across all cool season months. Conversely, CaRD10 reports more precipitation than observed in all cool season months and especially in December, February and March. This bias can be as high as 5 mm per day. Generally, CaRD10 matches the observation

well in terms of the seasonal distribution of SBJ events/days, Vmax, and precipitation.

Figure 12 shows interannual variations of SBJ events, SBJ days, Vmax, and

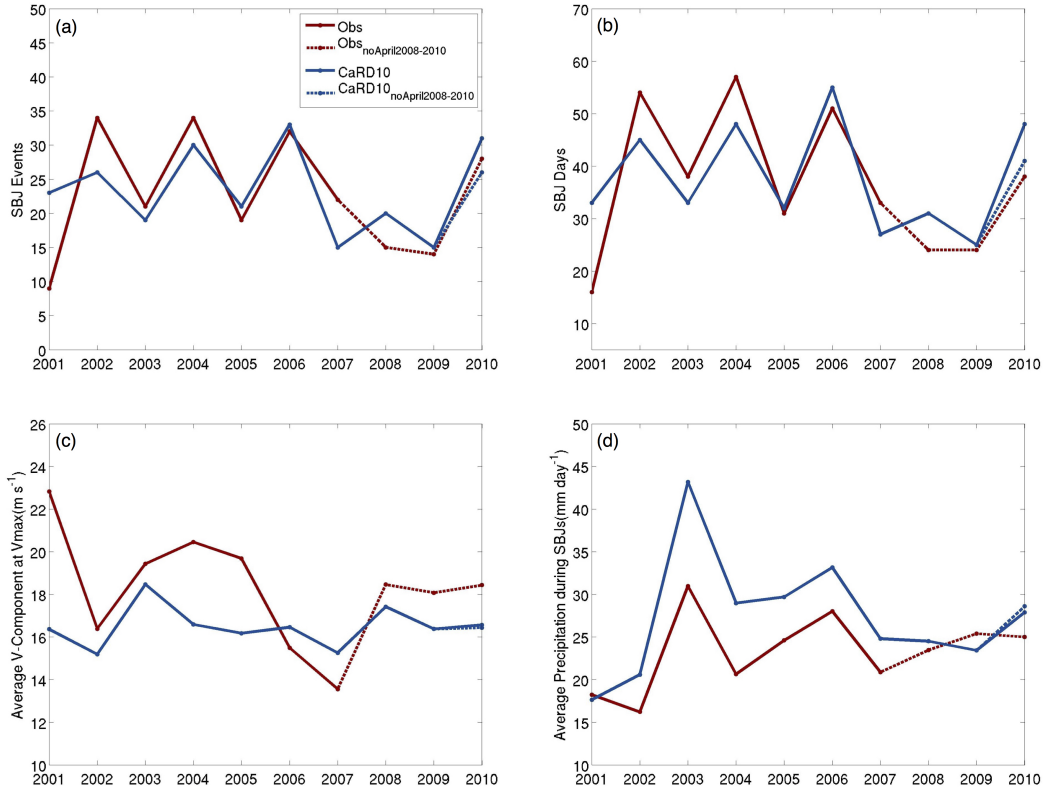

Figure 12: Cool season interannual variations of observed and CaRD10 at the grid closest to CCO from 2000 to 2010. (a) Number of SBJ events, (b) Number of SBJ days, (c) Average V-component at Vmax (m s^{-1}) and (d) Average precipitation of Region A during SBJs. Solid lines represent data from 2000 to 2007, October to April, dashed lines represent data from 2008 to 2010, October to March.

precipitation over Region A for observations and CaRD10. There is good agreement between CaRD10 and the observations for year-to-year variability in the number of SBJ events and days for most years. One notable exception is the cool season of 2000-2001, the numbers of SBJ events and days identified by CaRD10 are notably higher than observations, with 13 more events and 17 more days. For the Vmax and precipitation, CaRD10 also generally reproduces the observed interannual variations well. Although more SBJ events/days are identified by CaRD10 in 2001, the average precipitation during SBJs for

CaRD10 is nearly the same as observed. Note that CaRD10 shows much weaker Vmax (16 m s^{-1}) than the observed Vmax (23 m s^{-1}), which might affect the precipitation in Region A.

The preceding evaluation demonstrates that CaRD10 can realistically identify those SBJs with large magnitudes of Vmax, long durations, and associated with heavy precipitation in Region A during the SBJ period. In addition, CaRD10 also performs well in reproducing the seasonal cycle and year-to-year variability of SBJs. CaRD10 is an effective tool for us to study SBJs.

4.2 SBJ climatology and variability

Now that CaRD10 has been demonstrated to be able to identify SBJs, CaRD10 data from 1950 to 2012 is used to explore decadal variability and long-term trends of the number of SBJ events and days, SBJ duration, Vmax, and precipitation. Considering the importance of (El Nino-Southern Oscillation) ENSO and Pacific Decadal Oscillation (PDO) to precipitation over California (Schonher et al. 1989; Gershunov and Cayan 2003; Kirby et al. 2010; Hoell et al. 2015), the potential impact of ENSO and the PDO on SBJs is investigated.

Figure 13 shows the seasonal cycle of SBJs for the 1950-2012 period. SBJ events occur most frequently in December and second most frequently in January [Fig. 13]. The greatest number of SBJ days and the longest duration of SBJ events occur in January as well. In October and April, SBJs seldom appear, but the magnitude of Vmax and average daily precipitation in Region A do not decrease commensurately, which suggests that the SBJ wind speed and daily precipitation are not directly related with the frequency of SBJs among months.

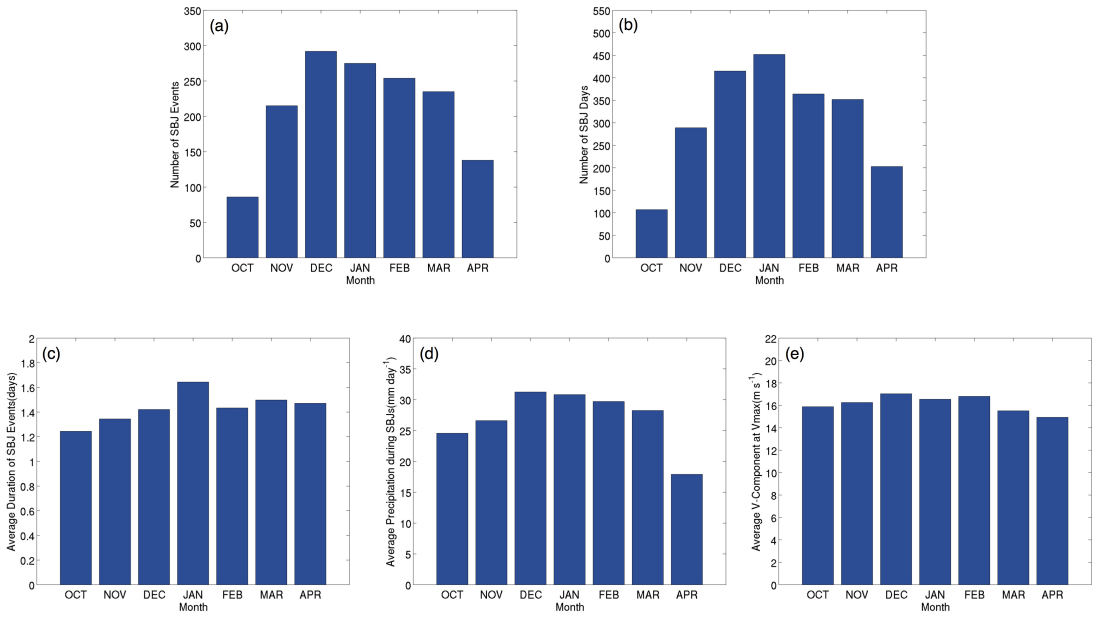

Figure 13: Cool season (October to April) monthly distributions of CaRD10 at the grid closest to CCO from 1951 to 2012. (a) Number of SBJ events, (b) Number of SBJ days, (c) Average duration of SBJ events (days), (d) Average V-component at Vmax (m $s-1$) and (e) Average precipitation of Region A during SBJs from 1950 to 2012.

Figure 14 shows interannual variability and long-term trends during 1950-2012 for SBJ events/days, SBJ duration, Vmax, average daily precipitation during SBJs, and total precipitation during the cool season in Region A. The linear trends for SBJ events/days, Vmax and total precipitation during the cool season are not statistically significant at the 95% level. For SBJ duration and average daily precipitation during SBJs, statistically significant increasing trends over time do occur. The SBJs tend to last longer in the latter part of the time period and thus may enhance precipitation in Region A.

The relationships between the number of SBJ events/days during the cool season and total cool season precipitation in Region A are also investigated. The correlation coefficients between number of SBJ events/days and total cool season precipitation are 0.784 and 0.827, respectively. These correlation values are statistically significant. To further show the correlations, scatter plots are shown in Fig. 15. The circles cluster near

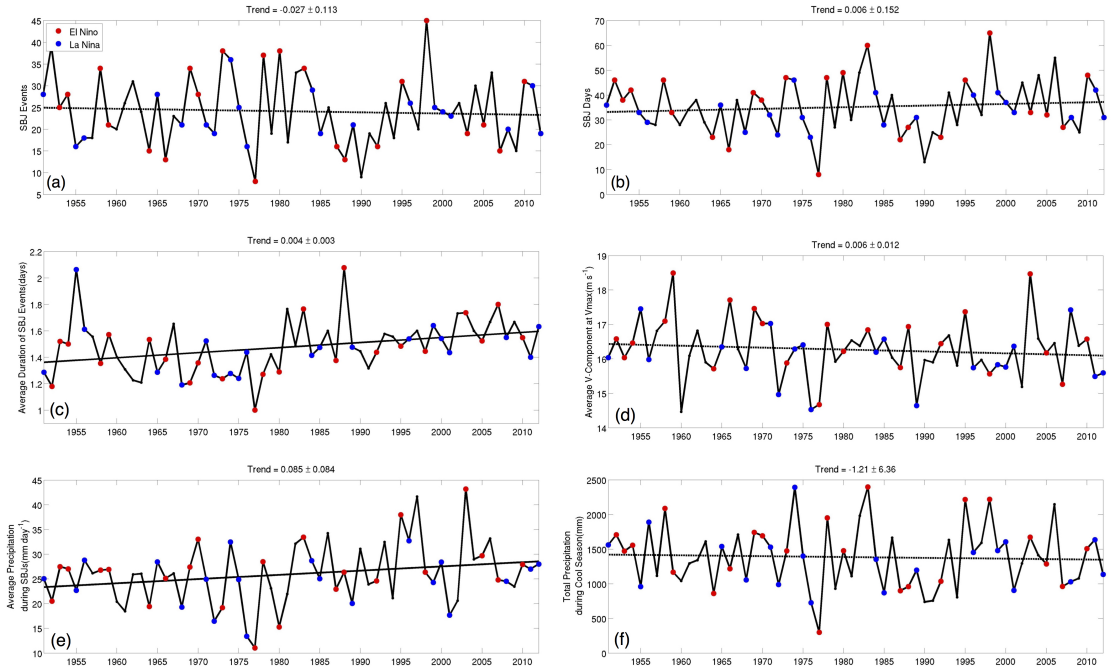

Figure 14: Cool season (October to April) interannual variations of CaRD10 at the grid closest to CCO from 1951 to 2012. (a) Number of SBJ events, (b) Number of SBJ days, (c) Average duration of SBJ events (days), (d) Average V-component at Vmax (m s^{-1}), (e) Average precipitation of Region A during SBJs and (f) Total precipitation of Region A during cool season from 1950 to 2012. The dashed black lines mark linear regression fits if not significant. The solid black lines mark significant linear regression fits. The red and blue dots show El-Nino and La-Nina year respectively.

the regression lines, showing an obvious linear relationship between the frequency of SBJ occurrences and total cool season precipitation.

It is interesting to note that the highest frequency of SBJ occurrence appears in 1998, which is one of the most far-reaching influential El Nino years. In order to figure out whether there is a general relationship between SBJs and ENSO, the El Nino years and La Nina years are marked by red dot and blue dots in Fig. 14. Visually there is no apparent relationship between El Nino or La Nina and the number of SBJ events and SBJ days in an individual cool season. Although many years with an extremely high frequency of SBJs and large Vmax are El Nino years, the daily precipitation in Region A during SBJs does not show the characteristic.

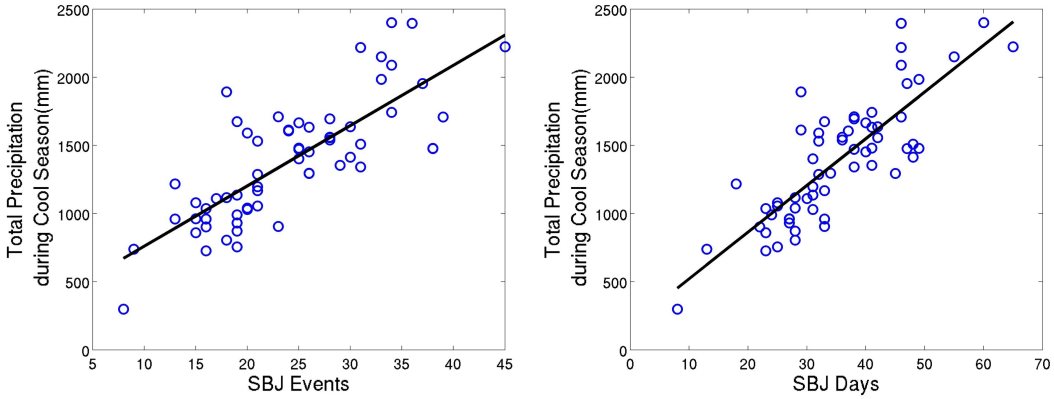

Figure 15: Scatter plots for relationship between (a) SBJ events and total precipitation during cool season, (b) SBJ days and total precipitation during cool season. The solid black lines show linear regression fits.

Moreover, the SBJ difference between El Nino years and La Nina years is

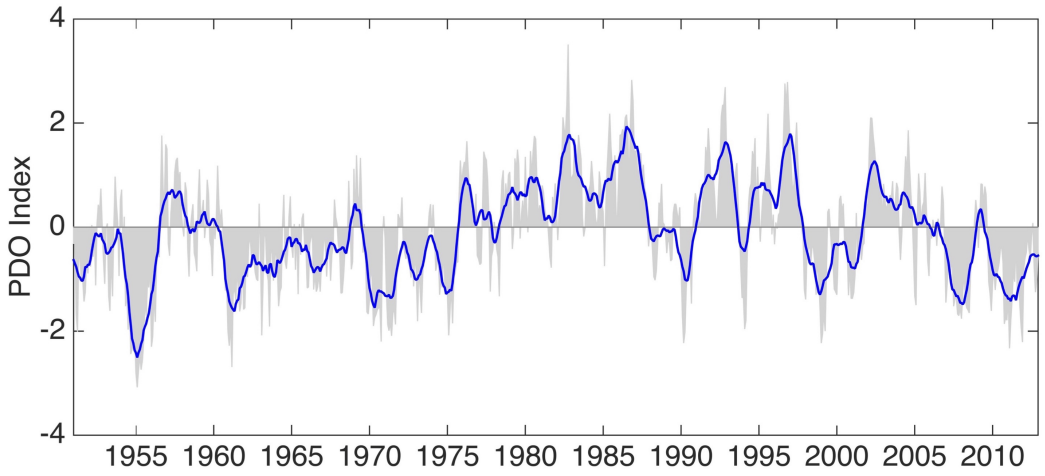

Figure 16: Monthly PDO index values (grey region) and 11-year running mean (blue line) from 1950 to 2012.

explored. Here only strong and moderate ENSO years are considered. There are 12 years for both El Nino and La Nina from 1950 to 2012. [Table. 7] The table shows average SBJ events/days, duration, Vmax and precipitation per year composited on El Nino years and La Nina years. During El Nino years, number of SBJ events per year is less than the one in La Nina year, while SBJ days quantity per year is a tiny larger. So the SBJ duration

during El Nino years is statistically longer than La Nina years. But SBJ the Vmax and related precipitation do not differ much, indicating that ENSO has little impact on SBJs.

The PDO is an El Nino-like long term ocean oscillatory pattern and more related with North Pacific region (Mantua 1999). According to Gershunov and Cayan (2003), Pacific climate modes are known to be responsible for climate variability and predictability in this region. The correlation between SBJ event number and PDO is explored. Their correlation coefficient does not far exceed the 95% confidence interval, suggesting that there is might no significant relationship between PDO and SBJ occurrences. More work need to be done to demonstrate that.

Chapter 5

Conclusion

In this study, the feasibility of using CaRD10 to identify SBJs is explored. CaRD10 was assessed with respect to SBJ wind profile, SBJ period and precipitation during SBJs from 2000 to 2010. In spite of overall negative bias of V component and exaggerated wind shear for some period, CaRD10 performs quite well at detecting strong wind speed and long duration SBJ events that are accompanied with substantial precipitation. In addition, CaRD10 realistically reproduces seasonal cycle and interannual variability of SBJ events/days, Vmax and precipitation in the north end of the Central Valley.

Although large variations among cool season months, the magnitudes of maximum Sierra-parallel component of flow are similar. Total precipitation over an individual cool season in the region north of the Central Valley is greater for those years with a greater number of SBJ events. Although experiencing substantial year-to-year variability, the average duration of SBJ events and the daily precipitation amount associated with SBJ events do exhibit statistically significant increasing trends. With simple investigation on the linkages of SBJs with (El Nino-Southern Oscillation) ENSO and Pacific Decadal Oscillation (PDO), no significant relationships are found.

The following work required to do is to fill the lack of April SBJ time from 2008 to 2010, thus more comprehensive evaluation for CaRD10 can be done. In the addition, more analyses are needed to demonstrate whether there is significant relationship between SBJs and ENSO and PDO. Besides, to fully understand the precipitation that related with SBJs, patterns of temperature under SBJ conditions need to be studied.

*This material currently is being prepared for submission for publication. Ms. Sun was the principal researcher/author on this paper. Sun, Chang; Norris, Joel. ”Using California Reanalysis Downscaling at 10 km to Identify the Sierra Barrier Jet and Its Variability since 1950”.

Bibliography

Carter, D., Gage, K., Ecklund, W., Angevine, W., Johnston, P., Riddle, A., Wilson, J., and Williams, C. (1995). Developments in uhf lower tropospheric wind profiling at noaa's aeronomy laboratory. *Radio Science*, 30(4):977–1001.

CNAP, CW3E, SWCSC, and DWR (2015). California precipitation.

Coulter, R. (2005). Radar wind profiler and rass (rwp915) handbook. Discussion paper, ARM TR-044.

Daly, C., Neilson, R. P., and Phillips, D. L. (1994). A statistical-topographic model for mapping climatological precipitation over mountainous terrain. *Journal of applied meteorology*, 33(2):140–158.

DWR (2015). Californias Most Significant Droughts: Comparing Historical and Recent Conditions.

DWR and USACE (2013). Californias Flood Future, Appendix B.

Fischler, M. A. and Bolles, R. C. (1981). Random sample consensus: a paradigm for model fitting with applications to image analysis and automated cartography. *Communications of the ACM*, 24(6):381–395.

Galewsky, J. and Sobel, A. (2005). Moist dynamics and orographic precipitation in northern and central california during the new year's flood of 1997. *Monthly weather review*, 133(6):1594–1612.

Gershunov, A. and Cayan, D. R. (2003). Heavy daily precipitation frequency over the contiguous united states: Sources of climatic variability and seasonal predictability. *Journal of Climate*, 16(16):2752–2765.

Gibson, J., Kallberg, P., Uppala, S., Hernandez, A., Nomura, A., and Serrano, E. (1997). Era description. ecmwf reanalysis project report series 1, european centre for medium range weather forecasts. *Reading, UK*, 66.

H. Kanamaru, Y. C. and Juang, H. (2005). Parallel implementation of the regional spectral atmospheric model. *PIER Project Rep*, page 23.

Hoell, A., Hoerling, M., Eischeid, J., Wolter, K., Dole, R., Perlwitz, J., Xu, T., and Cheng, L. (2015). Does el niño intensity matter for california precipitation? *Geophysical Research Letters*.

Hughes, M., Hall, A., and Fovell, R. G. (2009). Blocking in areas of complex topography, and its influence on rainfall distribution. *Journal of the Atmospheric Sciences*, 66(2):508–518.

Hughes, M., Neiman, P. J., Sukovich, E., and Ralph, M. (2012). Representation of the sierra barrier jet in 11 years of a high-resolution dynamical reanalysis downscaling compared with long-term wind profiler observations. *Journal of Geophysical Research: Atmospheres*, 117(D18).

Juang, H.-M. H. and Kanamitsu, M. (1994). The nmc nested regional spectral model. *Monthly Weather Review*, 122(1):3–26.

Kalnay, E., Kanamitsu, M., Kistler, R., Collins, W., Deaven, D., Gandin, L., Iredell, M., Saha, S., White, G., Woollen, J., et al. (1996). The ncep/ncar 40-year reanalysis project. *Bulletin of the American meteorological Society*, 77(3):437–471.

Kanamaru, H. and Kanamitsu, M. (2007). Fifty-seven-year california reanalysis downscaling at 10 km (card10). part ii: comparison with north american regional reanalysis. *Journal of Climate*, 20(22):5572–5592.

Kanamitsu, M. and Kanamaru, H. (2007). Fifty-seven-year california reanalysis downscaling at 10 km (card10). part i: System detail and validation with observations. *Journal of Climate*, 20(22):5553–5571.

Kim, J. and Kang, H.-S. (2007). The impact of the sierra nevada on low-level winds and water vapor transport. *Journal of Hydrometeorology*, 8(4):790–804.

Kingsmill, D. E., Neiman, P. J., Moore, B. J., Hughes, M., Yuter, S. E., and Ralph, F. M. (2013). Kinematic and thermodynamic structures of sierra barrier jets and overrunning atmospheric rivers during a landfalling winter storm in northern california. *Monthly Weather Review*, 141(6):2015–2036.

Kirby, M., Lund, S., Patterson, W., Anderson, M., Bird, B., Ivanovici, L., Monarrez, P., and Nielsen, S. (2010). A holocene record of pacific decadal oscillation (pdo)-related hydrologic variability in southern california (lake elsinore, ca). *Journal of Paleolimnology*, 44(3):819–839.

Livneh, B., Rosenberg, E. A., Lin, C., Nijssen, B., Mishra, V., Andreadis, K. M., Maurer, E. P., and Lettenmaier, D. P. (2013). A long-term hydrologically based dataset of land surface fluxes and states for the conterminous united states: Update and extensions*,#. *Journal of Climate*, 26(23):9384.

Loescher, K. A., Young, G. S., Colle, B. A., and Winstead, N. S. (2006). Climatology of barrier jets along the alaskan coast. part i: Spatial and temporal distributions. *Monthly weather review*, 134(2):437–453.

Lundquist, J. D., Minder, J. R., Neiman, P. J., and Sukovich, E. (2010). Relationships between barrier jet heights, orographic precipitation gradients, and streamflow in the northern sierra nevada. *Journal of Hydrometeorology*, 11(5):1141–1156.

Mantua, N. J. and Hare, S. R. (2002). The pacific decadal oscillation. *Journal of oceanography*, 58(1):35–44.

Marwitz, J. D. (1983). The kinematics of orographic airflow during sierra storms. *Journal of the Atmospheric Sciences*, 40(5):1218–1227.

Monteverdi, J. and Null, J. (1997). El niño and california precipitation. *Western Region Technical Attachment*, (97-37):21.

Neiman, P. J., Hughes, M., Moore, B. J., Ralph, F. M., and Sukovich, E. M. (2013). Sierra barrier jets, atmospheric rivers, and precipitation characteristics in northern california: A composite perspective based on a network of wind profilers. *Monthly Weather Review*, 141(12):4211–4233.

Neiman, P. J., Ralph, F. M., White, A., Kingsmill, D., and Persson, P. (2002). The statistical relationship between upslope flow and rainfall in california's coastal mountains: Observations during caljet. *Monthly Weather Review*, 130(6):1468–1492.

Neiman, P. J., Sukovich, E. M., Ralph, F. M., and Hughes, M. (2010). A seven-year wind profiler-based climatology of the windward barrier jet along california's northern sierra nevada. *Monthly Weather Review*, 138(4):1206–1233.

Parish, T. R. (1982). Barrier winds along the sierra nevada mountains. *Journal of Applied Meteorology*, 21(7):925–930.

Pierrehumbert, R. and Wyman, B. (1985). Upstream effects of mesoscale mountains. *Journal of the atmospheric sciences*, 42(10):977–1003.

Ralph, F. M., Neiman, P. J., and Wick, G. A. (2004). Satellite and caljet aircraft observations of atmospheric rivers over the eastern north pacific ocean during the winter of 1997/98. *Monthly Weather Review*, 132(7):1721–1745.

Ralph, F. M., Neiman, P. J., Wick, G. A., Gutman, S. I., Dettinger, M. D., Cayan, D. R., and White, A. B. (2006). Flooding on california's russian river: Role of atmospheric rivers. *Geophysical Research Letters*, 33(13).

Reynolds, D. W. and Dennis, A. S. (1986). A review of the sierra cooperative pilot project. *Bulletin of the American Meteorological Society*, 67(5):513–523.

Schonher, T. and Nicholson, S. (1989). The relationship between california rainfall and enso events. *Journal of Climate*, 2(11):1258–1269.

Smith, B. L., Yuter, S. E., Neiman, P. J., and Kingsmill, D. (2010). Water vapor fluxes and orographic precipitation over northern california associated with a landfalling atmospheric river. *Monthly Weather Review*, 138(1):74–100.

Smolarkiewicz, P. K. and Rotunno, R. (1990). Low froude number flow past three-dimensional obstacles. part ii: Upwind flow reversal zone. *Journal of the Atmospheric Sciences*, 47(12):1498–1511.

Weber, B., Wuertz, D., Welsh, D., and McPeek, R. (1993). Quality controls for profiler measurements of winds and rass temperatures. *Journal of Atmospheric and Oceanic Technology*, 10(4):452–464.